THE JOURNAL OF BIOLOGICAL CHEMISTRY VOL. 290, NO. 14, pp. 9141–9149, April 3, 2015

The Crystal Structure of the PB2 Cap-binding Domain of Influenza B Virus Reveals a Novel Cap Recognition Mechanism*

Received for publication, January 7, 2015, and in revised form, February 8, 2015 Published, JBC Papers in Press, February 17, 2015, DOI 10.1074/jbc.M115.636464

Yong Liu[‡§], **Yongfeng Yang**[‡§], **Jialin Fan**[‡§], **Ruina He**[‡§], **Ming Luo**[¶], **and Xiaofeng Zheng**[‡§1]

From the [‡]*State Key Lab of Protein and Plant Gene Research and* [§]*Department of Biochemistry and Molecular Biology, School of Life Sciences, Peking University, Beijing 100871, China and* [¶]*Department of Chemistry, Georgia State University, Atlanta, Georgia 30302*

Background: $PB2_{cap}$ is critical for the initiation of influenza virus transcription.
Results: FluB $PB2_{cap}$ binds to GDP and m^7GDP utilizing unique structural features, which is corroborated by data from ITC.
Conclusion: FluB $PB2_{cap}$ has a unique cap recognition mechanism compared with FluA $PB2_{cap}$.
Significance: We characterize the cap recognition mechanism of FluB $PB2_{cap}$, consequently providing insight into inhibitor design targeting FluB $PB2_{cap}$.

The influenza RNA-dependent RNA polymerase is a core enzyme required for both transcription and replication of the virus RNA genome, making it a potential drug target for the influenza virus. To detect the feature of cap-dependent transcription of influenza B virus (FluB) polymerase, we determined the crystal structures of the wild-type FluB polymerase PB2 subunit cap-binding domain ($PB2_{cap}$) with bound GDP and the mutant FluB Q325F $PB2_{cap}$ with bound m^7GDP or GDP. These structures revealed that, distinct from influenza A virus (FluA) $PB2_{cap}$, the guanine and ribose moieties of substrates invert in FluB $PB2_{caps}$. Moreover, we characterized the substrate specificity and affinity of the $PB2_{caps}$ using isothermal titration calorimetry. FluB $PB2_{cap}$ has a weaker affinity for m^7GDP than FluA $PB2_{cap}$. Unlike FluA $PB2_{cap}$ that has a preference for m^7GDP in comparison with GDP, FluB $PB2_{cap}$ shows an analogous affinity for both substrates. Replacement of FluB PB2 Glu^{325} by Phe, the corresponding residue of FluA PB2, increased the binding affinity of FluB $PB2_{cap}$ for m^7GDP to a level approximate to that of FluA $PB2_{cap}$ and caused a significant higher affinity to GDP. This study indicated that FluB $PB2_{cap}$ has a unique cap recognition mechanism compared with FluA $PB2_{cap}$, providing molecular insight into inhibitor design targeting FluB $PB2_{cap}$.

The influenza virus is subdivided into three different categories: influenza A virus (FluA),[2] influenza B virus (FluB), and influenza C virus (FluC). FluA is well studied as it frequently causes both pandemic and seasonal influenza. FluB mainly infects humans as a cause of seasonal influenza and is also detected in seals (1, 2). As an important pathogen of influenza-associated hospitalizations, FluB infection causes influenza and even mortality in humans, predominantly in children (3–5). The report for influenza-associated pediatric mortality showed that FluB, as 26% of circulating influenza viruses, caused 38% of all influenza-associated pediatric deaths in the United States during 2010–2011 (6). The latest report from the World Health Organization FluNet showed that FluB is prevalent as 24.8% of the seasonal epidemics each year and co-circulates with certain subtypes of FluA, such as FluA (H3N2) (29.5%) and FluA (H1N1) pdm09 (16.5%) viruses. In contrast, FluC has a distant evolutionary relationship with FluA and FluB and causes rare but still severe flu and sometimes local epidemics (7).

FluB is a negative-sense RNA virus, and its eight viral genome RNA segments (vRNA) encode 11 proteins. PA, PB1, and PB2 subunits form the influenza RNA-dependent RNA polymerase for both transcription and replication of vRNA. In the host nucleus, the polymerase transcribes vRNA by the "cap-snatching" mechanism (8). In transcription, the cap-binding domain of PB2 ($PB2_{cap}$) binds to the 5′ cap structures of host pre-mRNAs (9), and then the cap, together with 10–13 nucleotides downstream of the cap, is cleaved off by the N-terminal endonuclease domain of PA (10, 11). Subsequently, the generated 5′-capped RNA fragment serves as the primer to synthesize viral mRNA by the PB1 subunit. As a milestone contribution, the newest work from Cusack and co-workers (12, 13) clarified the atomic level assembly mode of the whole polymerase, including PA, PB1, and PB2 subunits and the viral RNA promoter.

The N7-methyl group of guanine in the cap structure of eukaryotic mRNA is essential for FluA to prime transcription (14). However, FluB polymerase recognizes not only the N7-methyl group of guanine (m^7G-capped RNAs) but also the unmethylated GpppG-RNAs efficiently (15). Moreover, FluB polymerase is demonstrated to have a weaker cap binding activity than FluA polymerase (15). A study recently proved that

* This work was supported by Beijing Natural Science Foundation Grant 5152012, National Science Foundation of China Grants 31470754 and 31170709, and Doctoral Fund Grant 20130001130003 of the Ministry of Education of China.

The atomic coordinates and structure factors (codes 4OR4, 4OR6, and 4Q46) have been deposited in the Protein Data Bank (http://wwpdb.org/).

[1] To whom correspondence should be addressed: School of Life Sciences, Peking University, Beijing 100871, China. Tel.: 86-10-6275-5712; Fax: 86-10-6276-5913; E-mail: xiaofengz@pku.edu.cn.

[2] The abbreviations used are: FluA, influenza A virus; FluB, influenza B virus; FluC, influenza C virus; vRNA, viral genome RNA segments; $PB2_{cap}$, cap-binding domain of PB2; ITC, isothermal titration calorimetry; W1–W6, water molecules 1–6.

VX-787, which is an inhibitor targeting FluA PB2$_{cap}$, is active against FluA but not against FluB (16). Taken together, these data suggest that FluB functions differently from FluA during the cap binding process.

The structures of the cap recognition mechanism for FluA PB2$_{cap}$ have been extensively studied. The structure of FluA PB2$_{cap}$ (amino acids 318–483) was first determined by Stephen Cusack and co-workers (9), and the cap-binding pocket complex with the cap analog m^{7}GTP was characterized. Furthermore, the conservative characteristics of the cap-binding pocket were evaluated (17), and the unliganded structure was solved (17, 18). Recently, inhibitors targeting the PB2 cap-binding pocket were reported (19, 20). These efforts provided clear atomic information for FluA PB2$_{cap}$ and indicated that the conserved cap-binding pocket is indeed a potential drug target. However, because several key amino acids in the cap-binding pocket are different from those of FluA, how FluB PB2$_{cap}$ functions in the cap binding mechanism and whether the cap-binding pocket of FluB is also a suitable drug target still remain to be resolved. Most recently, the structure of the whole FluB polymerase without cap binding for PB2 subunit was reported (12). The substrate binding information is still necessary for understanding the cap recognition mechanism of FluB PB2$_{cap}$.

In this study, we first report the crystal structure of FluB Q325F PB2$_{cap}$ with bound m^{7}GDP. Compared with FluA PB2$_{cap}$, the structure reveals that the guanine and ribose moieties of m^{7}GDP invert, resulting in the N7-methyl group and hydroxyl group of guanine facing outward of the binding pocket. We then solved the crystal structures of wild-type FluB PB2$_{cap}$ and FluB Q325F PB2$_{cap}$ with bound GDP. Here GDP shows the same cap binding pattern as m^{7}GDP, and the side chain of Gln^{325} in FluB PB2$_{cap}$-GDP shows conformational flexibility. Moreover, we characterize the cap binding affinity and specificity of these FluB PB2 $_{caps}$ and compare them with the FluA PB2$_{cap}$ by isothermal titration calorimetry (ITC). Our results indicate that the FluB polymerase possesses a novel cap recognition mechanism.

MATERIALS AND METHODS

Cloning, Protein Expression, and Purification—The cDNA encoding amino acids 320–484 of FluB polymerase PB2 subunit was obtained from influenza B/Jiangxi/BV/2006.[3] The Q325F, W359H, and Y434H mutations (amino acids 320–484) were constructed using a QuikChange™ site-directed mutagenesis kit (Stratagene) and confirmed by DNA sequencing. FluB PB2$_{cap}$ (amino acids 318–484) that contains two more wild-type residues Gly^{318}-Leu^{319} at the N terminus was cloned and is designated as FluB PB2$_{cap}$ in the following text. The FluA PB2$_{cap}$ (amino acids 318–483) gene from influenza A/Puerto Rico/8/34 (H1N1) was cloned as described previously (17, 22). All the cDNAs were digested with NdeI and XhoI and inserted into the pET28a vector with a His$_6$ tag at the N terminus. The recombinant FluB PB2$_{cap}$ plasmids were overexpressed in *Escherichia coli* strain BL21(DE3), and FluA PB2$_{cap}$ was expressed in *E. coli* strain Rosetta(DE3). Cells were grown at 37 °C until an A_{600} of 0.8–1.0 was reached, and then the protein expressions were induced with 0.3 mM isopropyl D-1-thiogalactopyranoside (Sigma) at 18 °C overnight. Cells were then harvested in a binding buffer (50 mM Tris, pH 8.0, 500 mM NaCl) and lysed by sonication. The cell lysate was centrifuged twice at 38,900 × *g* at 4 °C for 30 min each. The supernatant was filtered with a 0.22-μm membrane and purified by metal affinity chromatography using a HiTrap chelating HP column (GE Healthcare). The FluB PB2$_{cap}$ and FluB Q325F PB2$_{cap}$ proteins were subjected to thrombin digestion at 4 °C overnight, whereas FluA PB2$_{cap}$ was digested at 22 °C for 1 h, and then proteins were applied to a nickel affinity column to remove the His tag and undigested protein followed by purification using Superdex 75 gel filtration chromatography (GE Healthcare). The FluB Q325F PB2$_{cap}$ was further purified by ion exchange chromatography using a Q column (GE Healthcare). The protein was then dialyzed against buffer containing 10 mM Tris, pH 8.0, 200 mM NaCl for crystal screening or buffer containing 10 mM HEPES, pH 7.4, 150 mM NaCl for isothermal titration calorimetry.

Crystallization—10 mg ml^{-1} FluB Q325F PB2$_{cap}$ proteins were incubated with 5 mM m^{7}GTP (Sigma) and 5 mM GDP (Sigma) separately on ice for 1 h. The crystals used for data collection were obtained via the sitting drop vapor diffusion method at 20 °C. The FluB Q325F PB2$_{cap}$ with m^{7}GTP grew crystal clusters from 0.2 M ammonium acetate, 0.1 M Tris, pH 8.5, 25% (w/v) PEG 3350 after approximately 2 weeks, and a single crystal was extracted for data collection. The crystal of FluB Q325F PB2$_{cap}$ with GDP grew from 0.15 M DL-malic acid, pH 7.0, 20% (w/v) PEG 3350 within 2–4 days. 10–12 mg ml^{-1} FluB PB2$_{cap}$ (amino acids 318–484) was incubated with 5 mM m^{7}GTP, 5 mM, and 10 mM m^{7}GDP (Sigma), and 5 mM GDP separately for crystal screening purposes, and only the crystal of FluB PB2$_{cap}$with GDP was obtained from 0.2 M sodium formate, 20% (w/v) PEG 3350 within 2 days.

Data Collection and Structure Determination—All of the x-ray diffraction data were collected at Shanghai Synchrotron Radiation Facility (China) beamline BL17U. The corresponding reservoir solutions with a gradient of 5 and 10% (v/v) glycerol as a cryoprotectant for crystals of FluB Q325F PB2$_{cap}$-m^{7}GDP and FluB Q325F PB2$_{cap}$-GDP and with 5% (v/v) glycerol for FluB PB2$_{cap}$-GDP were used. After soaking, the crystals were flash cooled in liquid nitrogen and maintained at 100 K in cooled nitrogen gas for data collection. All of the data were processed with HKL 2000. The FluB Q325F PB2$_{cap}$-m^{7}GDP crystal structure was solved by molecular replacement using Molrep in the CCP4 suite (23) with the H3N2 PB2$_{cap}$-m^{7}GTP structure (Protein Data Bank code 4EQK) used as a search model. The 424-loop was rebuilt manually in Coot (24). The FluB Q325F PB2$_{cap}$-GDP and FluB PB2$_{cap}$-GDP were solved with the FluB Q325F PB2$_{cap}$-m^{7}GDP structure used as a search model. All the initial structures were refined by REFMAC5 (25) and built in Coot (24). The structure model of FluB Q325F PB2$_{cap}$-GDP was further refined with the geometry restraints by the refinement program in PHENIX (26). The final models were assessed with the program PROCHECK (27). The final statistics for data collection and structure refinement are presented in Table 1.

Isothermal Titration Calorimetry—ITC was carried out at 20 °C with a MicroCal iTC$_{200}$ (MicroCal Inc.). All proteins were

[3] K. Qin, unpublished sequence.

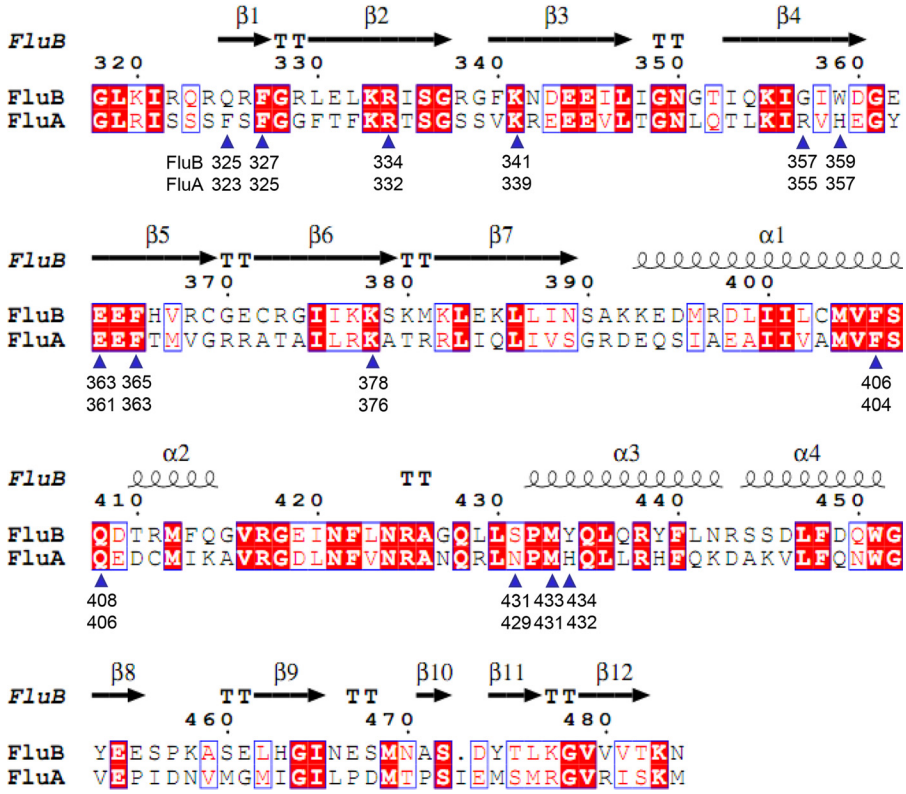

FIGURE 1. **Structure-based amino acid sequence alignments of FluB and FluA PB2$_{caps}$.** Amino acid sequence alignments of the PB2$_{caps}$, including FluA (influenza A/Puerto Rico/8/34 (H1N1)) and FluB (influenza B/Jiangxi/BV/2006), were analyzed by ESPript (37). The secondary structure and amino acid number of FluB PB2$_{cap}$-GDP are shown at the *top*. There are 14 residues associated with substrate binding in FluB or FluA PB2$_{caps}$ that are marked with *blue triangles*, and the respective amino acid number is noted for FluB and FluA PB2$_{caps}$.

desalted into a buffer containing 10 mM HEPES, pH 7.4, 150 mM NaCl with either m^{7}GDP or GDP dissolved in the same buffer. For FluA PB2$_{cap}$ and FluB PB2$_{cap}$, 240–280 μM protein (in the cell) and 2.5 mM m^{7}GDP or GDP (in the syringe) were used for titration. For FluB Q325F PB2$_{cap}$, 85 μM protein (in the cell) and 1.2 mM m^{7}GDP or GDP (in the syringe) were used. The first injection of 0.5 μl was followed by 34 injections of 1 μl with a 110-s spacer. All of the data were fitted to a single binding site model using Origin 7.0 program analysis.

RESULTS

The Crystal Structures of FluB Q325F PB2$_{cap}$ with Bound m^{7}GDP and GDP—Unlike FluA PB2$_{cap}$, FluB PB2$_{cap}$ readily precipitated out of solution at room temperature. During protein purification efforts, we noticed that the addition of m^{7}GTP improved the stability of FluB PB2$_{cap}$, which is similar to FluA PB2$_{cap}$. We obtained crystals of m^{7}GTP with FluA PB2$_{cap}$ (17) but not m^{7}GTP with FluB PB2$_{cap}$. Comparison of the residues of the cap-binding pocket between FluA and FluB revealed that the key difference(s) in the m^{7}GTP-binding site (cap-binding pocket) of PB2$_{cap}$ might result in the weak stability of FluB PB2$_{cap}$. Based on the sequence alignment (Fig. 1), Gln^{325}, Trp^{359}, and Tyr^{434} are the three key residues in the cap-binding pocket of FluB PB2$_{cap}$ that are different from FluA, and we thus mutated these residues to the corresponding residues of FluA PB2 (Q325F, W359H, and Y434H) and screened the three single mutations. FluB W359H PB2$_{cap}$ was insoluble, and FluB Y434H PB2$_{cap}$ exhibited the same instability as the wild type. However, FluB Q325F PB2$_{cap}$ showed greater stability than the wild type and was used for further crystallographic studies.

We first solved the crystal structure of FluB Q325F PB2$_{cap}$-m^{7}GTP at 2.21-Å resolution, and it was refined with an *R*-factor of 0.176 (R_{free} = 0.242) (Fig. 2*A* and Table 1). In the crystal structure, there was clear electron density for the substrate without the γ-phosphate observed (Fig. 3*B*), and we therefore named this structure as FluB Q325F PB2$_{cap}$-m^{7}GDP.

The structure of FluB Q325F PB2$_{cap}$-m^{7}GDP shares a similar conformation with FluA PB2$_{cap}$-m^{7}GTP (Protein Data Bank code 4EQK) with a 1.31-Å root mean square deviation mainly in the 424-loop and C-terminal loop (Fig. 2*B*). Surprisingly, FluB shows a distinct binding pattern to the substrate in the cap-binding pocket (Fig. 2, *C* and *D*). Compared with FluA PB2$_{cap}$-m^{7}GTP, the guanine moiety of m^{7}GDP in FluB Q325F PB2$_{cap}$ flips 180° around the long axis of the base, resulting in the N7-methyl group and hydroxyl group facing outward of the binding pocket and leaving room for a water molecule (W3) inside of the pocket. The broadened $F_o - F_c$ map (Fig. 3*A*, *green* map) suggests oscillation of the N7-methyl group, which may result because it points out into the solvent. In this case, Lys^{378} and Gln^{408} lose their interaction to the guanine moiety, whereas Arg^{334} forms a new 2.59-Å hydrogen bond with the hydroxyl group. Glu^{363} keeps conserved hydrogen bonds with the N1 and N2 of the guanine moiety. Trp^{359} sandwiches the methylated guanine moiety instead of His^{357} in FluA PB2$_{cap}$. Phe^{406} and Phe^{325} (the Q325F mutation) form the same upper

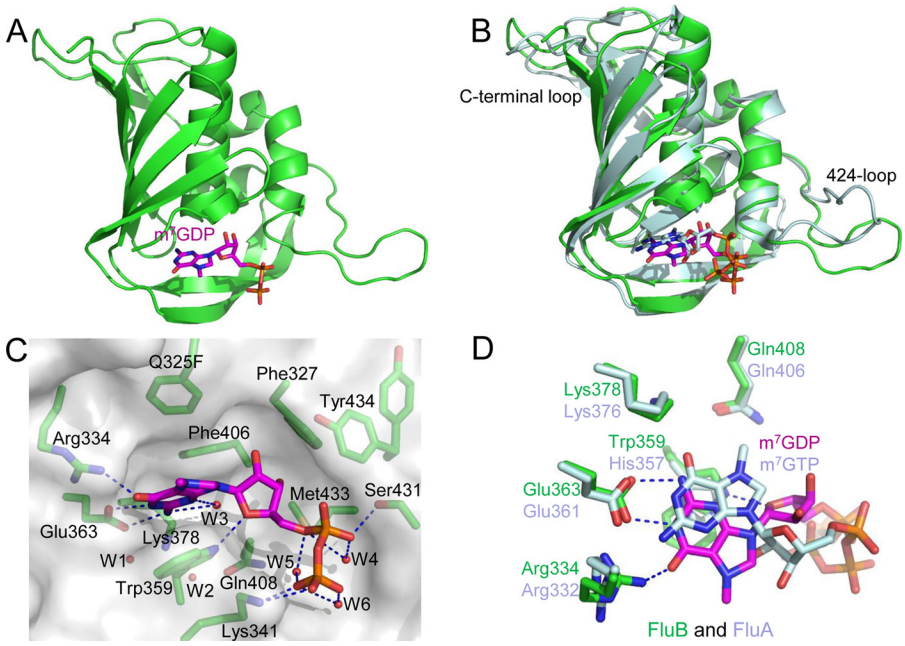

FIGURE 2. **Crystal structure of the FluB Q325F PB2$_{cap}$ with m^{7}GDP.** *A*, ribbon diagram of the structure of FluB Q325F PB2$_{cap}$-m^{7}GDP. The overall structure is in *green* with m^{7}GDP colored *purple*. *B*, structural superposition of FluB Q325F PB2$_{cap}$-m^{7}GDP (colored as in *A*) with FluA PB2$_{cap}$-m^{7}GTP (*pale cyan*; Protein Data Bank code 4EQK). *C*, close-up view of the cap-binding pocket of FluB Q325F PB2$_{cap}$-m^{7}GDP. Side chains are shown together with a *translucent* surface, and hydrogen bonds are indicated by *dotted lines*. Water molecules W1–W6 are presented as *red spheres*. *D*, comparison of the cap-binding pocket between FluB Q325F PB2$_{cap}$-m^{7}GDP and FluA PB2$_{cap}$-m^{7}GTP (colored as in *B*). The structure models in all figures were prepared with PyMOL (21).

TABLE 1

Data collection and refinement statistics

Mol/Asym, molecules per asymmetric unit; r.m.s., root mean square.

	Protein Data Bank code	4OR4	4OR6	4Q46
	Protein	FluB Q325F PB2$_{cap}$	FluB Q325F PB2$_{cap}$	FluB PB2$_{cap}$
	Ligand	m^{7}GDP	GDP	GDP
	Data collection			
	Space group	P $2_12_12_1$	P $2_12_12_1$	P 12_11
	Cell dimensions			
	a, *b*, *c* (Å)	42.94, 90.70, 95.77	42.97, 90.15, 95.71	43.07, 88.54 52.15
	α, β, γ (°)	90, 90, 90	90, 90, 90	90, 105.18, 90
	Mol/Asym	2	2	2
	Wavelength (Å)	0.9793	1.0000	0.9792
	Resolution (Å)	50-2.20 (2.24-2.20)	50-2.30 (2.30-2.36)	50-1.80 (1.83-1.80)[a]
	R_{merge} (%)[b]	16.0 (76.9)	21.2 (83.0)	7.7 (21.7)
	I/σ	22.6 (4.6)	10.9 (3.8)	19.9 (8.5)
	Completeness (%)	99.9 (100)	99.9 (99.9)	94.6 (98.2)
	Redundancy	7.8 (7.9)	9.3 (9.3)	5.5 (5.3)
	Refinement			
	Resolution (Å)	42.35-2.21	30.13-2.29	24.57-1.80
	No. reflections	19,227	17,022	31,459
	R_{work}/R_{free} (%)[c]	17.6/24.2	18.5/25.0	17.0/23.0
	Average B-factors (Å^2)	26.84	25.22	18.0
	Protein (chain A, B)	27.02, 25.88	25.54, 24.37	16.51,17.77
	Ligand (chain A, B)	21.87, 24.53	20.59, 22.85	13.79, 14.01
	Water	34.91	30.94	30.91
	r.m.s. deviations			
	Bond lengths (Å)	0.022	0.002	0.025
	Bond angles (°)	2.197	0.614	2.170
	Ramachandran plot (%)			
	Favored region	97.5	96.9	98.5
	Allowed region	2.5	3.1	1.5
	Outlier region	0	0	0

[a] Numbers in parentheses are for highest resolution shell.
[b] $R_{merge} = \Sigma|I_i - I|/\Sigma|I_i|$.
[c] $R = \Sigma h|F_o(h) - F_c(h)|/\Sigma|hF_o(h)|$. R_{free} is calculated using 5% of the data excluded from the refinement.

cover as FluA PB2$_{cap}$ for stacking interactions to the guanine moiety (Fig. 3, *A* and *C*). Phe^{325} has a 4.52-Å distance to the N7 of the guanine moiety (Fig. 3*A*) compared with the 3.4-Å distance between Phe^{404} and the N7-methyl group in FluA PB2$_{cap}$ (Fig. 3*C*). The ribose moiety is also inverted in the structure, and the ribose hydroxyl groups face inward toward the pocket and are close to Phe^{327} and Met^{433}. The O4 of the ribose moiety forms a 2.85-Å hydrogen bond with Trp^{359}. Although the guanine and ribose moieties invert, the diphosphate moiety of m^{7}GDP shows a similar trend as that of m^{7}GTP in FluA PB2$_{cap}$.

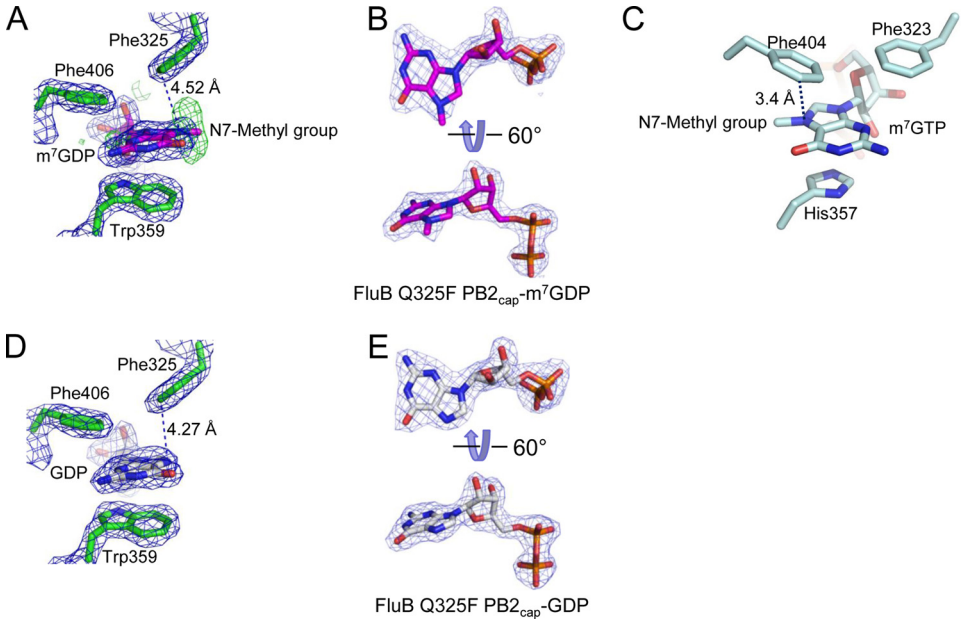

FIGURE 3. **Comparison of the cap-binding pockets of FluB Q325F PB2$_{cap}$ with m^{7}GDP and GDP, and FluA PB2$_{cap}$-m^{7}GTP.** *A* and *B*, electron density of the cap-binding pocket of molecule A of FluB Q325F PB2-m^{7}GDP (*purple*) with the vertical $F_o - F_c$ map (*green*) of the N7-methyl group in *A* and the $2F_o - F_c$ map (*blue*) of single m^{7}GDP in *B*. *C*, the cap-binding pocket of FluA PB2$_{cap}$-m^{7}GTP. Phe^{323}, His^{357}, and Phe^{404} are shown to bind m^{7}GTP. *D* and *E*, electron density of the cap-binding pocket of molecule A of FluB Q325F PB2-GDP (*white*) in *D* with the electron density of single GDP in *E*. The *dotted lines* in *A*, *C*, and *D* point to the shortest distance between Phe^{325} and N7 of m^{7}GDP/GDP/m^{7}GTP. The $2F_o - F_c$ (*blue*) and $F_o - F_c$ (*green*; in *A*) maps contoured at 1.4 and 2.5 σ, respectively, were generated by the FFT program in CCP4 (23) and drawn by PyMOL (21).

The diphosphate moiety of m^{7}GDP forms hydrogen bonds with Ser^{431} (α-phosphate, 2.78 Å) and Lys^{341} (β-phosphate, 2.69 and 3.18 Å) with three well ordered water molecules internally placed (W4, W5, and W6). Tyr^{434} loses its interaction with the substrate, whereas in FluA PB2$_{cap}$, His^{432} binds to the α-phosphate of the m^{7}GTP at the corresponding position. As found in the FluA PB2$_{caps}$ structure (9, 17), there are also two water molecules (W1 and W2) that are buried among residues Glu^{363}, Lys^{378}, and Gln^{408}.

The FluB polymerase recognizes both the m^{7}G-capped RNAs and the unmethylated GpppG-RNAs efficiently (15). The structure of FluB Q325F PB2$_{cap}$-m^{7}GDP shows the N7-methyl group pointing out toward the solvent. To test whether the unmethylated GpppG-RNA binds in the same orientation, we determined the crystal structure of GDP-bound FluB Q325F PB2$_{cap}$. The crystal structure of FluB Q325F PB2$_{cap}$-GDP was obtained within 2–4 days after co-crystallization with 5 mM GDP. The 2.29-Å FluB Q325F PB2$_{cap}$-GDP structure was refined with an *R*-factor of 0.185 (R_{free} = 0.250) (Table 1). In the cap-binding pocket here, GDP shows the same conformation as m^{7}GDP in FluB Q325F PB2$_{cap}$-m^{7}GDP (Fig. 3, *D* and *E*).

Gln^{325} Is Flexible in the Cap-binding Pocket of Wild-type FluB PB2$_{cap}$—The structure of the wild-type FluB PB2$_{cap}$ with its substrate is essential for understanding how the wild-type residue Gln^{325} interacts with substrate. As mentioned above, we failed to crystallize FluB PB2$_{cap}$ with m^{7}GTP even though the addition of m^{7}GTP improved the stability of FluB PB2$_{cap}$. Based on the successful crystallization of FluB Q325F PB2$_{cap}$ with m^{7}GDP and GDP, we further screened the crystals of wild-type FluB PB2$_{cap}$ with m^{7}GDP and GDP. We obtained crystals and solved the structure of FluB PB2$_{cap}$ (amino acids 318–484) bound with GDP but not with the methylated substrate m^{7}GDP.

The structure of FluB PB2$_{cap}$-GDP was solved to 1.8-Å resolution and refined with an *R*-factor of 0.170 (R_{free} = 0.230) (Fig. 4, *A* and *B*, and Table 1). The GDP in the structure (Fig. 4, *C* and *D*) shows the same orientation as the GDP and m^{7}GDP in FluB Q325F PB2$_{cap}$ (Fig. 3, *D* and *A*). There are two molecules in the crystallographic asymmetric unit. In molecule B, the side chain of Gln^{325} shows a 3.96-Å distance to GDP (Fig. 4*D*), and in molecule A, the side chain of Gln^{325} is disordered with weak electron density (Fig. 4*C*). These observations suggest that Gln^{325} is flexible and may contribute weakly to cap binding of FluB PB2$_{cap}$.

Structural analysis revealed that the N7-methyl group is oscillating in FluB Q325F PB2$_{cap}$-m^{7}GDP (Fig. 3*A*) and that Gln^{325} in the wild-type FluB PB2$_{cap}$ is more flexible than Phe^{325} of the mutant (Fig. 4*C*). These data may explain why we could not obtain the crystal of FluB PB2$_{cap}$-m^{7}GDP. Based on the crystal structures solved in this investigation, we propose a model for wild-type FluB PB2$_{cap}$ binding to m^{7}GDP (Fig. 4*E*). In the model, m^{7}GDP keeps the same orientation as m^{7}GDP in the crystal structure of FluB Q325F PB2$_{cap}$-m^{7}GDP (Fig. 3*A*) and is consistent with GDP in FluB Q325F PB2$_{cap}$-GDP (Fig. 3*D*) and FluB PB2$_{cap}$-GDP (Fig. 4, *C* and *D*). The orientation of Gln^{325} is the same as that of Gln^{325} in FluB PB2$_{cap}$-GDP (Fig. 4*D*) and is similar to that of Phe^{325} in FluB Q325F PB2$_{cap}$-m^{7}GDP (Fig. 3*A*) and FluB Q325F PB2$_{cap}$-GDP (Fig. 3*D*). All three available crystal structures and the model presented here show that the guanine and ribose moieties of substrates invert in FluB PB2$_{caps}$ compared with those of FluA PB2$_{cap}$.

FluB and FluA PB2$_{caps}$ Show Different Substrate Specificity and Affinity—To investigate the cap binding affinity resulting from the structural differences between FluB and FluA PB2$_{caps}$, we examined the affinity of m^{7}GDP and GDP to FluA, FluB, and FluB Q325F PB2$_{caps}$ using ITC, respectively (Fig. 5). ITC was

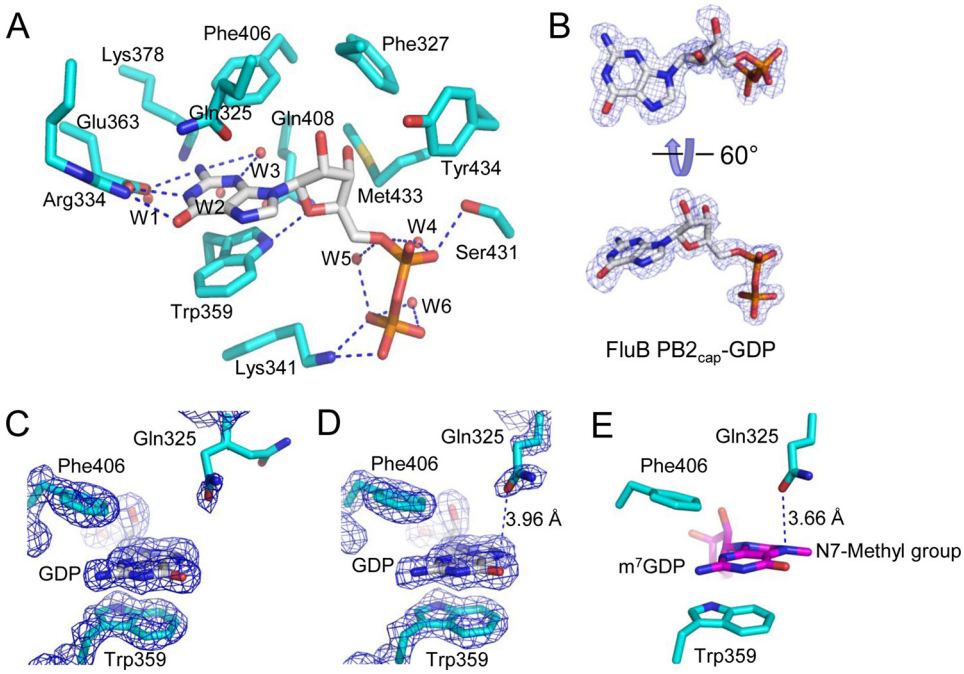

FIGURE 4. **Crystal structure of the cap-binding pocket of FluB PB2$_{cap}$-GDP.** *A*, close-up view of the cap-binding pocket of FluB PB2$_{cap}$-GDP (FluB PB2$_{cap}$ is colored *cyan*, and GDP is colored *white*). *B*, electron density of GDP in molecule A of FluB PB2$_{cap}$-GDP. *C* and *D*, electron density of the cap-binding pockets of molecule A (*C*) and molecule B (*D*) of FluB PB2$_{cap}$-GDP. *E*, proposed structural model of FluB PB2 binding m^{7}GDP based on the structures shown in Figs. 3, *A* and *C*, and 4*D*. The *dotted lines* in *D* and *E* point to the shortest distance between Gln^{325} and N7 of GDP/m^{7}GDP. The $2F_o - F_c$ (*blue*) map contoured at 1.4 σ was generated by the FFT program in CCP4 (23) and drawn by PyMOL (21).

carried out at 20 °C in a buffer containing 10 mM HEPES, pH 7.4, 150 mM NaCl. Consistent with previous reports (9), FluA PB2$_{cap}$ was favored a methylated substrate with a dissociation equilibrium constant (K_d) of 17 μM for m^{7}GDP and 118 μM for GDP. In contrast, FluB PB2$_{cap}$ showed an approximated binding to m^{7}GDP (167 μM) and GDP (169 μM) with about one-tenth of the affinity of FluA PB2$_{cap}$ to m^{7}GDP and slightly weaker affinity to GDP than FluA PB2$_{cap}$. Notably, the Q325F mutation significantly improves the affinity of FluB PB2$_{cap}$ to both m^{7}GDP (26.8 μM; 6.2-fold) and GDP (4.9 μM; 34.5-fold) and shows great specificity for GDP *versus* m^{7}GDP. Compared with FluA PB2$_{cap}$, FluB Q325F PB2$_{cap}$ shows a similar affinity to m^{7}GDP and tighter binding characteristics to GDP. These results indicate that FluB PB2$_{cap}$ possesses different substrate specificity and affinity compared with those of FluA PB2$_{cap}$.

DISCUSSION

Influenza B virus has a devastating mortality rate in humans, especially in children (3, 4, 6), which is an essential characteristic of seasonal influenza. Structural information for FluB PB2$_{cap}$, a core executor for the transcription initiation of influenza polymerase, had previously been unknown. The structure of the whole FluB polymerase was reported recently; however, it still lacks substrate binding information for cap snatching (12). Whether FluB PB2$_{cap}$ functions with the same cap binding mechanism as FluA is unclear. Conversely, the neuraminidase structures of FluA and FluB viruses show a common drug-binding pocket (28); therefore, FluB can be treated with the same clinical drugs, such as oseltamivir (Tamiflu®) and zanamivir (Relenza®), as FluA. As a potential drug target, whether FluB PB2$_{cap}$ and FluA PB2$_{cap}$ can bind to the same inhibitors is currently unknown. Herein, we have determined the structures of substrate-binding FluB PB2$_{cap}$ and FluB Q325F PB2$_{cap}$ and characterized their substrate specificity and affinity.

Our results suggest that, unlike FluA PB2$_{cap}$, FluB PB2$_{cap}$ has a novel cap recognition feature. In both structures of FluB wild-type and Q325F PB2$_{caps}$, the guanine and ribose moieties of m^{7}GDP (GDP) invert around the long axis of the base compared with FluA PB2$_{cap}$, leaving the N7-methyl group and hydroxyl group of the guanine moiety facing outward and the ribose hydroxyl group facing toward the cap-binding pocket (Fig. 2). According to the structure and sequence alignments between FluA and FluB Q325F PB2$_{caps}$ (Figs. 1 and 2*D*), this inversion may be caused by the orientation of Trp^{359} in FluB PB2$_{caps}$, whereas a His^{357} occupies the same position of FluA PB2$_{cap}$.

Lys^{378} and Gln^{408} of FluB PB2$_{cap}$ lose their interactions with m^{7}GDP (GDP) due to the inversion of the guanine moiety, consistent with the report that these two residues contribute less to cap binding (15). Conversely, Arg^{334} of FluB PB2$_{cap}$ is a newly identified residue utilized for the recognition of the outward facing hydroxyl group of guanine moiety that functions similarly to Lys^{376} in FluA PB2$_{cap}$ (at the corresponding position of Lys^{378} of FluB PB2$_{cap}$; Figs. 1 and 2*D*). Conservatively, Glu^{363} of FluB PB2$_{cap}$ retains recognition of N1 and N2 of guanine moiety as in FluA (Figs. 1 and 2*D*). In conclusion, the available structural information for PB2$_{caps}$ indicates that both FluA and FluB need an acidic glutamate and an alternative basic residue for the recognition of the guanine moiety in the cap-snatching mechanism (Fig. 2*D*).

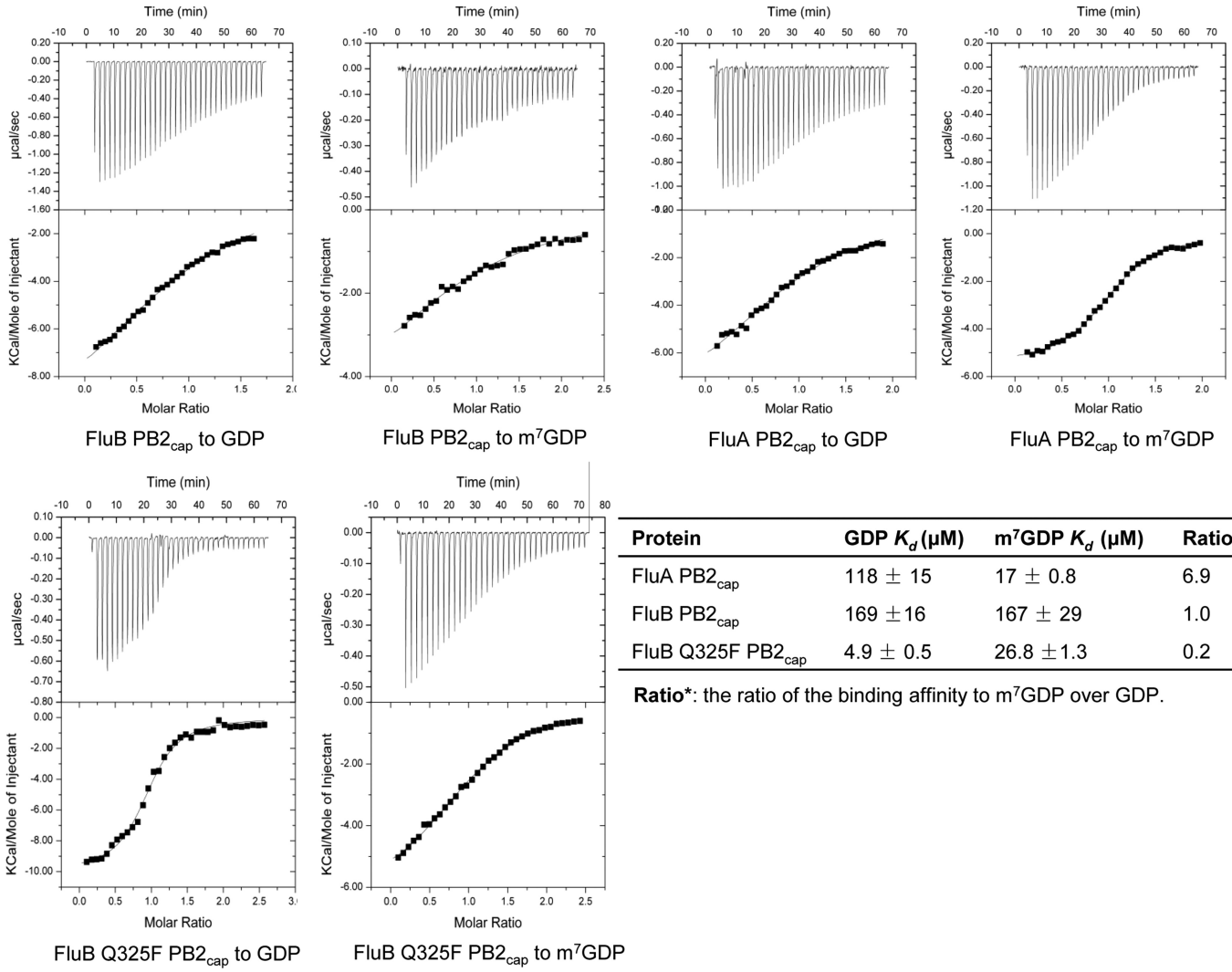

Protein	GDP K_d (µM)	m^{7}GDP K_d (µM)	Ratio*
FluA PB2$_{cap}$	118 ± 15	17 ± 0.8	6.9
FluB PB2$_{cap}$	169 ±16	167 ± 29	1.0
FluB Q325F PB2$_{cap}$	4.9 ± 0.5	26.8 ±1.3	0.2

Ratio*: the ratio of the binding affinity to m^{7}GDP over GDP.

FIGURE 5. **Comparison of the substrate specificity and affinity between FluA, FluB and FluB Q325F PB2$_{caps}$ by ITC.** The binding of FluA PB2$_{cap}$, FluB PB2$_{cap}$, and FluB Q325F PB2$_{cap}$ to m^{7}GDP and GDP was analyzed by ITC. The raw data are depicted in the *top panels* with the integrated data in the *bottom panels*. All data are shown with continuous lines fitting to a one-site binding model. The dissociation equilibrium constants (K_d) are listed in the table. The standard errors of affinity represent data fitted to binding isotherms in the *lower panel*.

The combination of Trp^{359}, Phe^{406}, and Gln^{325} is used to clamp the guanine moiety and is associated with the weak cap binding of FluB PB2$_{cap}$ to m^{7}GDP. In contrast, the mutation Q325F can recover the affinity of FluB PB2$_{cap}$ to m^{7}GDP (Fig. 5). The weak cap binding affinity of methylated substrate to FluB PB2$_{cap}$ could further explain why the RNA elongation and cap binding activities of the FluB polymerase are lower than those of the FluA polymerase (15). However, it is unclear whether some other factors contribute to the unexpectedly low affinity of the FluB PB2$_{cap}$ to substrates under physiological conditions.

The inversion of the guanine moiety also allows FluB PB2$_{cap}$ to accept GDP well. The ITC results revealed that FluB PB2$_{cap}$ has an equal affinity for GDP and m^{7}GDP (Fig. 5). The side chain of Gln^{325} shows conformational flexibility in molecule A of FluB PB2$_{cap}$-GDP (Fig. 4*C*). These observations suggest that the flexibility of Gln^{325} may contribute to the weak recognition of the N7-methyl and unmethylated substrates.

In contrast, both FluB Q325F PB2$_{cap}$ and FluA PB2$_{cap}$ could distinguish m^{7}GDP from GDP (Fig. 5) because Phe^{325} in FluB Q325F PB2$_{cap}$ and Phe^{404} in FluA PB2$_{cap}$ are used for rigid packing to the N7-methyl group (Fig. 3, *A* and *C*). In a comparison of FluA PB2 with FluB PB2, FluB PB2 could recognize GpppG for cap primer generation, although it fails in elongation (15). It has been reported that the transcript from the non-methylated cap primer could not be translated by host ribosomes (29–31). Whether the recognition of non-methylated cap primer by FluB has a physiological role is unclear; therefore further investigation is needed.

Cap-binding proteins in humans, such as the heterodimeric nuclear cap-binding complex (32) and eIF4E (33), show a higher affinity to methylated substrates and significant discrimination against non-methylation (34–36). Therefore, the cap recognition of FluB PB2$_{cap}$ for both m^{7}GDP and GDP with a low affinity provides a good opportunity for rational inhibitor design. First, the binding cavity allows FluB PB2$_{cap}$ to accommodate both GDP and m^{7}GDP derivatives. Second, a modification of N3 of the guanine moiety, such as the addition of a hydroxyl to N3 (Protein Data Bank code 3G9L), may recover its interaction with Lys^{378} and Gln^{408}. FluA PB2$_{cap}$ may also utilize

this modification, which has the potential to interact with Arg^{332} of FluA $PB2_{cap}$ (Fig. 2*D*). Third, N7 of the guanine moiety could be modified to interact with Gln^{325}. Finally, modification of the ribose hydroxyl groups facing inward toward the pocket is likely to build a stronger interaction to Tyr^{434} or Phe^{327}. In summary, our data have provided the structural and biochemical basis for cap recognition of FluB $PB2_{cap}$, which in turn helps in understanding how FluB $PB2_{cap}$ executes the cap binding process and provides further insight into rational inhibitor design targeting FluB $PB2_{cap}$.

Acknowledgments—We thank Dr. Kun Qin for providing the cDNA of influenza virus. We also thank the staff at the Shanghai Synchrotron Radiation Facility beamline BL17U and the Beijing Synchrotron Radiation Facility beamline 3W1A for assistance in data collection and Drs. Tao Jiang, Sheng Ye, and Yun Zhu at the Institute of Biophysics, Chinese Academy of Sciences; Zhaoyang Ye at Peking University; and Zengqiang Gao at the Beijing Synchrotron Radiation Facility for assistance with crystal testing and data collection. We also thank Dr. Lorenzo Finci and Linglong Qu (Peking University) for careful editing of the manuscript.

REFERENCES

1. Osterhaus, A. D., Rimmelzwaan, G. F., Martina, B. E., Bestebroer, T. M., and Fouchier, R. A. (2000) Influenza B virus in seals. *Science* **288,** 1051–1053
2. Bodewes, R., Morick, D., de Mutsert, G., Osinga, N., Bestebroer, T., van der Vliet, S., Smits, S. L., Kuiken, T., Rimmelzwaan, G. F., Fouchier, R. A., and Osterhaus, A. D. (2013) Recurring influenza B virus infections in seals. *Emerg. Infect. Dis.* **19,** 511–512
3. McCullers, J. A., and Hayden, F. G. (2012) Fatal influenza B infections: time to reexamine influenza research priorities. *J. Infect. Dis.* **205,** 870–872
4. Paddock, C. D., Liu, L., Denison, A. M., Bartlett, J. H., Holman, R. C., Deleon-Carnes, M., Emery, S. L., Drew, C. P., Shieh, W. J., Uyeki, T. M., and Zaki, S. R. (2012) Myocardial injury and bacterial pneumonia contribute to the pathogenesis of fatal influenza B virus infection. *J. Infect. Dis.* **205,** 895–905
5. Thompson, W. W., Shay, D. K., Weintraub, E., Brammer, L., Bridges, C. B., Cox, N. J., and Fukuda, K. (2004) Influenza-associated hospitalizations in the United States. *JAMA* **292,** 1333–1340
6. Centers for Disease Control and Prevention (CDC) (2011) Influenza-associated pediatric deaths—United States, September 2010-August 2011. *MMWR. Morb. Mortal. Wkly. Rep.* **60,** 1233–1238
7. Roy Mukherjee, T., Mukherjee, A., Mullick, S., and Chawla-Sarkar, M. (2013) Full genome analysis and characterization of influenza C virus identified in Eastern India. *Infect. Genet. Evol.* **16,** 419–425
8. Plotch, S. J., Bouloy, M., Ulmanen, I., and Krug, R. M. (1981) A unique cap(m7GpppXm)-dependent influenza virion endonuclease cleaves capped RNAs to generate the primers that initiate viral RNA transcription. *Cell* **23,** 847–858
9. Guilligay, D., Tarendeau, F., Resa-Infante, P., Coloma, R., Crepin, T., Sehr, P., Lewis, J., Ruigrok, R. W., Ortin, J., Hart, D. J., and Cusack, S. (2008) The structural basis for cap binding by influenza virus polymerase subunit PB2. *Nat. Struct. Mol. Biol.* **15,** 500–506
10. Yuan, P., Bartlam, M., Lou, Z., Chen, S., Zhou, J., He, X., Lv, Z., Ge, R., Li, X., Deng, T., Fodor, E., Rao, Z., and Liu, Y. (2009) Crystal structure of an avian influenza polymerase PA(N) reveals an endonuclease active site. *Nature* **458,** 909–913
11. Dias, A., Bouvier, D., Crépin, T., McCarthy, A. A., Hart, D. J., Baudin, F., Cusack, S., and Ruigrok, R. W. (2009) The cap-snatching endonuclease of influenza virus polymerase resides in the PA subunit. *Nature* **458,** 914–918
12. Reich, S., Guilligay, D., Pflug, A., Malet, H., Berger, I., Crépin, T., Hart, D., Lunardi, T., Nanao, M., Ruigrok, R. W., and Cusack, S. (2014) Structural insight into cap-snatching and RNA synthesis by influenza polymerase. *Nature* **516,** 361–366
13. Pflug, A., Guilligay, D., Reich, S., and Cusack, S. (2014) Structure of influenza A polymerase bound to the viral RNA promoter. *Nature* **516,** 355–360
14. Bouloy, M., Plotch, S. J., and Krug, R. M. (1980) Both the 7-methyl and the 2′-O-methyl groups in the cap of mRNA strongly influence its ability to act as primer for influenza virus RNA transcription. *Proc. Natl. Acad. Sci. U.S.A.* **77,** 3952–3956
15. Wakai, C., Iwama, M., Mizumoto, K., and Nagata, K. (2011) Recognition of cap structure by influenza B virus RNA polymerase is less dependent on the methyl residue than recognition by influenza A virus polymerase. *J. Virol.* **85,** 7504–7512
16. Byrn, R. A., Jones, S. M., Bennett, H. B., Bral, C., Clark, M. P., Jacobs, M. D., Kwong, A. D., Ledeboer, M. W., Leeman, J. R., McNeil, C. F., Murcko, M. A., Nezami, A., Perola, E., Rijnbrand, R., Saxena, K., Tsai, A. W., Zhou, Y., and Charifson, P. S. (2015) Preclinical activity of VX-787, a first in class, orally bioavailable inhibitor of the influenza virus polymerase PB2 subunit. *Antimicrob. Agents Chemother.* **59,** 1569–1582
17. Liu, Y., Qin, K., Meng, G., Zhang, J., Zhou, J., Zhao, G., Luo, M., and Zheng, X. (2013) Structural and functional characterization of K339T substitution identified in the PB2 subunit cap-binding pocket of influenza A virus. *J. Biol. Chem.* **288,** 11013–11023
18. Tsurumura, T., Qiu, H., Yoshida, T., Tsumori, Y., Hatakeyama, D., Kuzuhara, T., and Tsuge, H. (2013) Conformational polymorphism of m^7GTP in crystal structure of the PB2 middle domain from human influenza A virus. *PLoS One* **8,** e82020
19. Clark, M. P., Ledeboer, M. W., Davies, I., Byrn, R. A., Jones, S. M., Perola, E., Tsai, A., Jacobs, M., Nti-Addae, K., Bandarage, U. K., Boyd, M. J., Bethiel, R. S., Court, J. J., Deng, H., Duffy, J. P., Dorsch, W. A., Farmer, L. J., Gao, H., Gu, W., Jackson, K., Jacobs, D. H., Kennedy, J. M., Ledford, B., Liang, J., Maltais, F., Murcko, M., Wang, T., Wannamaker, M. W., Bennett, H. B., Leeman, J. R., McNeil, C., Taylor, W. P., Memmott, C., Jiang, M., Rijnbrand, R., Bral, C., Germann, U., Nezami, A., Zhang, Y., Salituro, F. G., Bennani, Y. L., and Charifson, P. S. (2014) Discovery of a novel, first-in-class, orally bioavailable azaindole inhibitor (VX-787) of influenza PB2. *J. Med. Chem.* **57,** 6668–6678
20. Pautus, S., Sehr, P., Lewis, J., Fortuné, A., Wolkerstorfer, A., Szolar, O., Guilligay, D., Lunardi, T., Décout, J. L., and Cusack, S. (2013) New 7-methylguanine derivatives targeting the influenza polymerase PB2 cap-binding domain. *J. Med. Chem.* **56,** 8915–8930
21. DeLano, W. L. (2010) *The PyMOL Molecular Graphics System*, Version 1.3r1, Schrödinger, LLC, New York
22. Liu, Y., Meng, G., Luo, M., and Zheng, X. (2013) Crystallization and x-ray crystallographic analysis of the cap-binding domain of influenza A virus H1N1 polymerase subunit PB2. *Acta Crystallogr. Sect. F Struct. Biol. Cryst. Commun.* **69,** 280–283
23. Collaborative Computational Project, Number 4 (1994) The CCP4 suite: programs for protein crystallography. *Acta Crystallogr. D Biol. Crystallogr.* **50,** 760–763
24. Emsley, P., and Cowtan, K. (2004) Coot: model-building tools for molecular graphics. *Acta Crystallogr. D Biol. Crystallogr.* **60,** 2126–2132
25. Murshudov, G. N., Vagin, A. A., and Dodson, E. J. (1997) Refinement of macromolecular structures by the maximum-likelihood method. *Acta Crystallogr. D Biol. Crystallogr.* **53,** 240–255
26. Adams, P. D., Afonine, P. V., Bunkóczi, G., Chen, V. B., Davis, I. W., Echols, N., Headd, J. J., Hung, L. W., Kapral, G. J., Grosse-Kunstleve, R. W., McCoy, A. J., Moriarty, N. W., Oeffner, R., Read, R. J., Richardson, D. C., Richardson, J. S., Terwilliger, T. C., and Zwart, P. H. (2010) PHENIX: a comprehensive Python-based system for macromolecular structure solution. *Acta Crystallogr. D Biol. Crystallogr.* **66,** 213–221
27. Morris, A. L., MacArthur, M. W., Hutchinson, E. G., and Thornton, J. M. (1992) Stereochemical quality of protein structure coordinates. *Proteins* **12,** 345–364
28. Taylor, N. R., Cleasby, A., Singh, O., Skarzynski, T., Wonacott, A. J., Smith, P. W., Sollis, S. L., Howes, P. D., Cherry, P. C., Bethell, R., Colman, P., and Varghese, J. (1998) Dihydropyrancarboxamides related to zanamivir: a new series of inhibitors of influenza virus sialidases. 2. Crystallographic

and molecular modeling study of complexes of 4-amino-4H-pyran-6-carboxamides and sialidase from influenza virus types A and B. *J. Med. Chem.* **41,** 798–807

29. Graff, J. R., and Zimmer, S. G. (2003) Translational control and metastatic progression: enhanced activity of the mRNA cap-binding protein eIF-4E selectively enhances translation of metastasis-related mRNAs. *Clin. Exp. Metastasis* **20,** 265–273
30. von der Haar, T., Gross, J. D., Wagner, G., and McCarthy, J. E. (2004) The mRNA cap-binding protein eIF4E in post-transcriptional gene expression. *Nat. Struct. Mol. Biol.* **11,** 503–511
31. Culjkovic, B., Topisirovic, I., and Borden, K. L. (2007) Controlling gene expression through RNA regulons: the role of the eukaryotic translation initiation factor eIF4E. *Cell Cycle* **6,** 65–69
32. Mazza, C., Segref, A., Mattaj, I. W., and Cusack, S. (2002) Large-scale induced fit recognition of an m^{7}GpppG cap analogue by the human nuclear cap-binding complex. *EMBO J.* **21,** 5548–5557
33. Marcotrigiano, J., Gingras, A. C., Sonenberg, N., and Burley, S. K. (1997) Cocrystal structure of the messenger RNA 5′ cap-binding protein (eIF4E) bound to 7-methyl-GDP. *Cell* **89,** 951–961
34. Kinkelin, K., Veith, K., Grünwald, M., and Bono, F. (2012) Crystal structure of a minimal eIF4E-Cup complex reveals a general mechanism of eIF4E regulation in translational repression. *RNA* **18,** 1624–1634
35. Rosettani, P., Knapp, S., Vismara, M. G., Rusconi, L., and Cameron, A. D. (2007) Structures of the human eIF4E homologous protein, h4EHP, in its m7GTP-bound and unliganded forms. *J. Mol. Biol.* **368,** 691–705
36. Osborne, M. J., Volpon, L., Kornblatt, J. A., Culjkovic-Kraljacic, B., Baguet, A., and Borden, K. L. (2013) eIF4E3 acts as a tumor suppressor by utilizing an atypical mode of methyl-7-guanosine cap recognition. *Proc. Natl. Acad. Sci. U.S.A.* **110,** 3877–3882
37. Robert, X., and Gouet, P. (2014) Deciphering key features in protein structures with the new ENDscript server. *Nucleic Acids Res.* **42,** W320–W324